Available online at www.sciencedirect.com
SCIENCE DIRECT®
Scripta Materialia 50 (2004) 1193–1198
Scripta MATERIALIA
www.actamat-journals.com

Micromechanical analysis on residual stress-induced nanoindentation depth shifts in DLC films

Yun-Hee Lee [a,b,*], Kazuki Takashima [a], Dongil Kwon [b]

[a] Precision and Intelligence Laboratory, Tokyo Institute of Technology, 4259 Nagatsuta, Midori-ku, Yokohama 226-8503, Japan
[b] School of Materials Science and Engineering, Seoul National University, San 56-1, Gwanak-gu, Seoul 151-742, South Korea

Received 28 November 2003; received in revised form 3 February 2004; accepted 5 February 2004

Abstract

A depth change in nanoindentation curve by an influence of elastic residual stress was modeled as a reversible surface deformation by adopting an elastic contact mechanics for a flat punch. The model, however, yielded overestimated stresses for two diamond-like carbon films. The discrepancy was discussed from a viewpoint of irreversible deformation around the punch.

Keywords: Diamond-like carbon film; Nanoindentation; Residual stresses

1. Introduction

A thin film has residual stress due to an existence of discontinuous interface, inhomogeneous thermal history during deposition or subsequent fabrication process, and various imperfections by ion bombardment [1,2]. The residual stress has significant influences on mechanical property and reliability of the thin film and thin-film based microdevice. Thus several measuring methods [2,3] have been developed but still have difficulties in sample preparation, testing procedure, and data analysis. Thus a nanoindentation technique was recently proposed as an alternative [4]. The technique is insightful as a stress-probing method of the thin film because it has been developed for a microsized sample and several elastic and plastic properties can be analyzed from the raw data simultaneously [5,6]. Although early studies [7,8] tried to derive a dependency of an apparent hardness on applied stress, alteration in the hardness by the elastic stress was less than 10% of its value in the unstressed specimen. Tsui et al. [9,10], studying a effect of surface stress on indenting plasticity by investigating both a shape of the indentation curve and remnant contact impressions, reported that hardness was invariant regardless of the elastic residual stress. Suresh and Giannakopoulos [11] tried to analyze the surface stress from the difference in contact area of stressed and unstressed materials at a fixed depth. Several studies [12,13] were followed to find a stress-indicating indentation parameter from sharp and spherical indentations.

Recently Lee and Kwon [4] developed a contact model for analyzing the residual stress from a load shift in the indentation curve based on a unique stress interaction concept and its validity was confirmed through some experimental studies [14,15]. Furthermore an influence of biaxial surface stress on the indentation deformation was assessed by a model modification with a stress-directionality parameter [16]. In this study, we explore a new micromechanical modeling on a difference in the indentation depth, overlooked in previous studies [4,11,14], of as-deposited and free-standing films at a fixed load. In order to express the stress-induced depth shift in terms of the residual stress, such concepts as the elastic stress-independent hardness [9,10], elastic punching mechanics [5,17], and stress interaction based on shear plasticity [4,14–16] are incorporated into a step-by-step analysis.

2. Theoretical model

2.1. Effects of thin-film stress on indentation curve and contact morphology

A compressive surface stress produces an indentation loading curve stiffer than that in stress-free state by

* Corresponding author. Address: Precision and Intelligence Laboratory, Tokyo Institute of Technology, 4259 Nagatsuta, Midori-ku, Yokohama 226-8503, Japan. Tel./fax: +81-459245631.
E-mail address: uni44@mmrl.snu.ac.kr (Y.-H. Lee).

1359-6462/$ - see front matter
doi:10.1016/j.scriptamat.2004.02.009

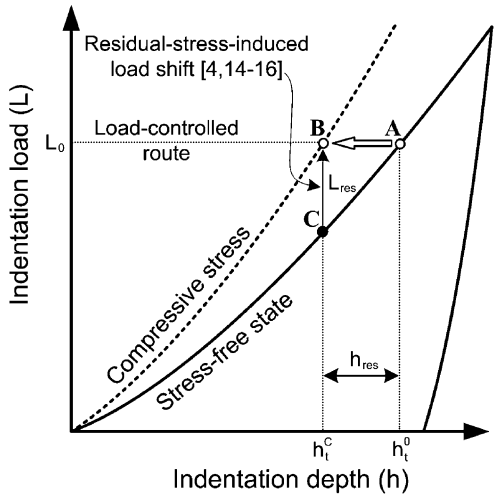

Fig. 1. Influences of the compressive stress on the shift behaviors in the indentation loading curve.

decreasing a contact shear stress. Significant changes in the indentation loading curve by application of the compressive stress in Fig. 1 can be scrutinized from two viewpoints. One is a stress-induced load shift L_{res} at a prescribed indentation depth h_t^{C} (a shift from point C to point B) and its theoretical analysis has been carried out in previous studies [4,14–16]. The other is a stress-induced depth shift $h_t^0 - h_t^{\text{C}}$ or h_{res} at a fixed indentation load L_0 (a shift from point A to point B). However, there was no attempt to analyze h_{res} because a depth parameter could not be easily related to a stress or load parameter. In this study, a definition of L_{res} [4,14] and an elastic contact analysis for a flat punch [5,17] was combined to analyze the stress-induced depth shift h_{res}. A basic assumption used is that the hardness is independent of the elastic residual stress [9,10]. To satisfy the assumption, two triangular contact regions in Fig. 2 must be identical at the fixed load regardless of the stress state. Thus the difference in the indentation depth $h_t^0 - h_t^{\text{C}}$ or h_{res} is solely attributed to a surface deformation around the contact.

2.2. Micromechanical analysis on the contact morphology in the stressed state

The indentation depth h_t^0 is considered as a sum of a true contact depth h_{C}^0 and an elastic surface deflection h_{S}^0 around the contact (right part in Fig. 2) [17]. h_{S}^0 is expressed as $\omega L_0/S_0$ according to the Oliver–Pharr analysis [6], where the indenter geometry constant ω is 0.72 for a sharp indenter and S_0 is the contact stiffness. The linear dependency of h_{S}^0 on L_0, agreeing to the elastic contact behavior around a flat punch, can be rearranged as Eq. (1) by expressing S_0 in terms of a true contact area A_{C}^0 and reduced Young's modulus E_r.

$$h_{\text{S}}^0 = \frac{\sqrt{\pi}\omega L_0}{2E_r\sqrt{A_{\text{C}}^0}}. \tag{1}$$

A contact morphology in the compressive stress state can be inferred from already-known facts of the stress-induced depth shift, assumption of the elastic stress-independent hardness [9,10], and its corresponding morphology in the stress-free state. In order to simultaneously satisfy a smaller indentation depth h_t^{C} and the same contact depth h_{C}^0 at the prescribed load L_0 comparing to those of the stress-free state, a characteristic feature in the compressive stress state should be a pile-up deformation h_p around the contact (see the left part in Fig. 2). If the contact morphology of the stress-free state reversibly converges to that in the compressive stress state by an elastic stress application along the load-controlled route in Fig. 1, the indentation depth will decrease from h_t^0 to h_t^{C} by a formation of the stress-induced pile-up deformation. Since this procedure maintains the contact area as invariant according to the elastic stress-independent hardness, the elastic defor-

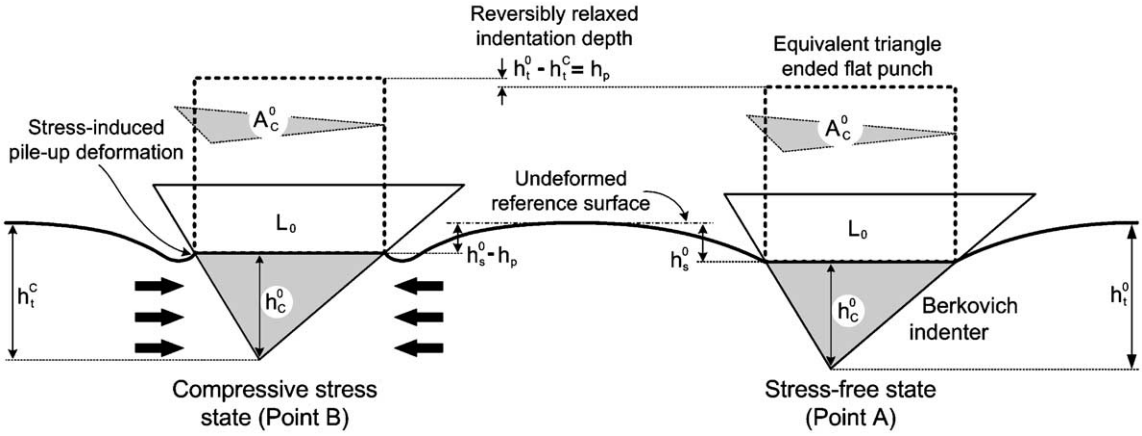

Fig. 2. Changes in the contact morphology at a fixed load by the application of the elastic stress and their approximations as elastic contact deformations around flat punches.

mation in the indentation depth can be approximated as a reversible surface response around an equivalent flat punch in Fig. 2. To express the surface deformation in the compressive stress state with Eq. (1), it is important to find an equivalent state of point B on the indentation loading curve in the stress-free state; the indentation depth h_t^C of point B corresponds to point C, having a lower punch load $L_0 - L_{res}$ in the stress-free state (see Fig. 2). Thus the surface elastic deformation $h_S^0 - h_p$ in Fig. 2 could be expressed as

$$h_S^0 - h_p = \frac{\sqrt{\pi}\omega(L_0 - L_{res})}{2E_r\sqrt{A_C^0}}. \quad (2)$$

The residual stress-induced normal load L_{res} is already defined as $2\sigma^{res}A_C^0/3$ for the equi-biaxial compressive stress according to the previous study [4,14]. Note that L_{res} in the compressive stress has the opposite sign of Ref. [4] and h_p has a same magnitude of $h_t^0 - h_t^C$ (refer to Figs. 1 and 2). Thus an equation for the thin-film stress can be derived as Eq. (3) by subtracting Eq. (1) from Eq. (2) with the definition of L_{res}.

$$\sigma^{res} = -\frac{3E_r}{\omega\sqrt{\pi A_C^0}}(h_t^0 - h_t^C). \quad (3)$$

3. Experimental details

Two kinds of 0.4 and 0.6 μm-thick DLC thin films were deposited on Si wafers using radio-frequency plasma-assisted chemical vapor deposition (R.F. PACVD) with C_6H_6 source gas [14]. The reaction pressure and the bias voltage were 10 mtorr and −400 V, respectively. Average surface roughness measured by an atomic force microscope (AFM) were 8.6 ± 3.1 nm and 1.8 ± 1.3 nm for the 0.4 and 0.6 μm-thick DLC films, respectively. 5×5 mm samples for the nanoindentation tests were cut from the whole deposited wafers. A free-standing film in the stress-free state was fabricated by removing the Si substrate with 60% HNO_3+30% HF + 10% CH_3COOH aqueous solution [14]. The free-standing film was rinsed with ethyl-alcohol, placed and slightly pressed on a bare Si base without an adhesive, and subsequently indented. A plastic work-hardening of the free-standing film during the handling is neglected due to its brittleness.

Nanoindentation tests were performed using Triboscope (made by Hysitron, Inc.) with depth and load resolutions of 0.1 nm and 0.1 μN, respectively. The indenter was also used as an AFM tip and the specimen surface was imaged immediately before indentation to locate the indenter on a smoother region less than 4.0 nm. Maximum indentation depth was determined to be less than 1/10 of the film thickness, thus excluding the effect of the substrate deformation. The indentation loads satisfying this condition were 1000 and 2000 μN for the 0.4 and 0.6 μm-thick DLC films, respectively. To select reliable indentation curves from the center of the raw data, more than 10 nanoindentation tests were repeated for each thin film with a loading speed of 250 μN/s using a Berkovich indenter.

4. Results and discussion

4.1. Nanoindentation data for the as-deposited and free-standing films

The raw load-depth curves of the as-deposited films were reproducible; the measured indentation depths at the peak load were overlapped within a standard deviation of ±0.4 nm. Two kinds of the raw nanoindentation curve were obtained for the stress-free films; one group showed a general loading behavior similar to that of the as-deposited film, while the other, showing low repeatability, had an erroneous inflection point. The inflection, detected by a differentiation of the loading curve with respect to the depth, is attributed to a slight air gap between the free-standing film and Si base [18]. If a local bulged region in the free-standing film is tested, the indenter will probe a low load increment behavior before a rapid contact loading by a bending of the floated film (see a trend of asterisk symbol in Fig. 3(a)). The indentation curves selected for the free-standing films also showed a good reproducibility within a standard deviation of ±0.3 nm at the peak load. All nanoindentation curves selected from the as-deposited and free-standing films were superposed in Fig. 3. The indentation curves for the as-deposited film (solid symbols) showed a leftward shift comparing with those of the free-standing film (open symbols), representing a compressive residual stress in the DLC thin films.

4.2. Hardness and Young's modulus of the diamond-like carbon film

Contact depth h_C^{max}, analyzed from the nanoindentation curve in the free-standing film through an Oliver–Pharr method [6], was converted to contact area A_C^{max} at the peak load using an empirically calibrated geometry function of the Berkovich indenter. The contact depth, hardness, and reduced Young's modulus without the effect of the residual stress were, respectively, 27.3 ± 0.4 nm, 3.67 ± 0.19 GPa, and 75.41 ± 1.15 GPa for the 0.4 μm-thick DLC film. The corresponding properties for the 0.6 μm-thick DLC film were 27.1 ± 0.3 nm, 24.13 ± 0.44 GPa, and 287.34 ± 3.91 GPa, respectively. To estimate the thin-film stress at several load steps, a contact depth corresponding to each selected load must be predicted from the contact data of the final unloading curve. The reduced Young's modulus E_r is expressed as

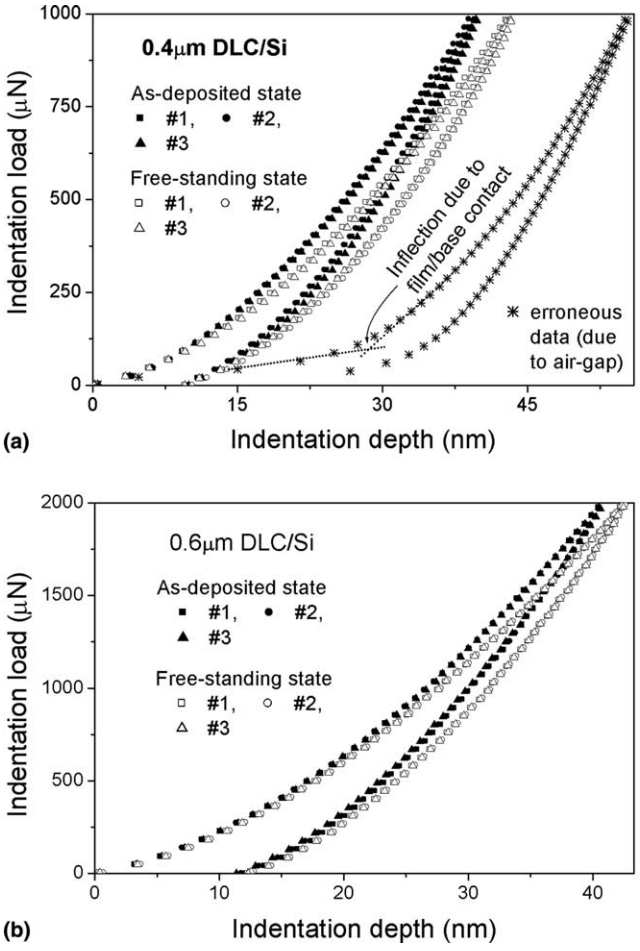

Fig. 3. Shape change in the indentation curves for (a) 0.4 μm and (b) 0.6 μm-thick DLC thin films arising from the residual stress.

a function of the indentation load L_0 and contact depth h_C^0 from Eq. (1). Note that h_S^0 and A_C^0 are, respectively, expressed as $h_t^0 - h_C^0$ and the empirical polynomial function of h_C^0. Thus if the intrinsic value of E_r and L_0 are given, the corresponding contact depth h_C^0 can be easily determined through a numerical iteration method (see Table 1).

4.3. Thin-film stress estimated through the load-controlled stress model

Nanoindentation loading curves of the as-deposited and free-standing films in Fig. 3 were fitted into a power-law function of the depth or $L = k_L h^{m_L}$, where k_L and m_L are fitting constants (see Table 2). Then the residual stress was estimated using Eq. (3) with the information of E_r, h_C^0, and $h_t^0 - h_t^C$, determined from Table 2 by inserting the analyzing load L_0. The resulting stresses were -1.29 ± 0.10 and -3.92 ± 0.29 GPa, respectively, for the 0.4 and 0.6 μm-thick DLC films. These are, however, 20–30% higher than the stress values estimated in the previous study [14] for the same samples; the actual stress levels for the 0.4 and 0.6 μm-thick DLC films were -1.08 ± 0.05 and -3.04 ± 0.16 GPa, respectively. The discrepancy might be explained from an irreversible deformation zone extended outside of the contact in the free-standing film.

Table 1
Contact depths calculated at several load steps for two DLC films in the free-standing state

0.4 μm-thick DLC film		0.6 μm-thick DLC film	
Load (μN)	Contact depth (nm)	Load (μN)	Contact depth (nm)
1000	27.3 ± 0.4	2000	27.1 ± 0.3
800	23.4	1800	24.7
600	19.1	1400	19.6
400	14.0	1000	14.1

Table 2
Power-law fittings of the loading curves for the as-deposited and free-standing films

Thin film	Stress state	k_L	m_L
0.4 μm DLC/Si	As-deposition	2.262 ± 0.073	1.653 ± 0.014
	Free-standing	2.151 ± 0.080	1.623 ± 0.007
0.6 μm DLC/Si	As-deposition	5.695 ± 0.112	1.577 ± 0.006
	Free-standing	5.607 ± 0.267	1.564 ± 0.014

The elastic contact mechanics of the flat punch [5,17] was adopted in describing the surface deformation around the actual indentation on the DLC film with the Berkovich indenter. This implies that the irreversibly deformed zone is constrained beneath the flat punch regardless of the stress state and that the elastic surface deformations of points A* and B disappear and converge to the reference surface of point F with decreasing the punch load (see elastic routes A*–F and B–F in Fig. 4). Note that points A and B are corresponding to those in Fig. 1. However, since a resistance of the free-standing film to the irreversible deformation is much lower than its as-deposited counterpart [19], the indentation-induced plastic zone can extend outside of the contact region (see point A) and an irreversible punch depth h_{res}^{irr} exists after the load-controlled stress-relaxation (see point F* in Fig. 4). Since an actual punching deformation of the free-standing film follows an elastic/plastic loading F–A and elastic unloading A–F* routes, the irreversible punch depth h_{res}^{irr} is measured from a difference in the contact depth from the as-deposited and free-standing films. The contact depth of the as-deposited film also can be measured using the Oliver–Pharr method [6] because no residual-stress-induced plastic deformation occurs at the perimeter of the contact and the elastic residual stress does not alter the elastic contact theory of the flat punch. The contact depths at the peak loads were 26.1 ± 0.4 and 26.6 ± 0.2 nm for the 0.4 and 0.6 μm-thick DLC films in as-deposited state, respectively, and their corresponding irreversible punch

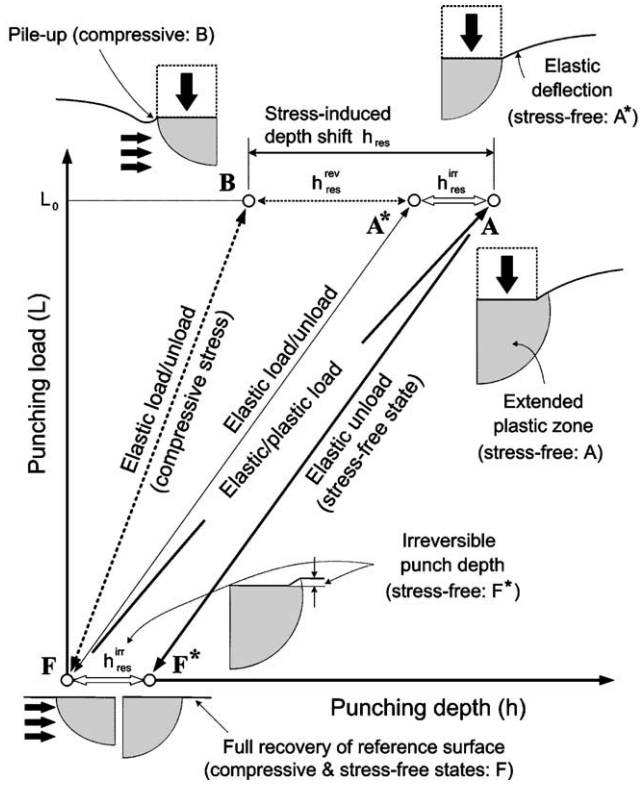

Fig. 4. Measurement of the irreversible deformation around the flat punch $h_{\mathrm{res}}^{\mathrm{irr}}$ and its influence on the whole stress-induced depth shift h_{res}.

depths were 1.2 and 0.5 nm. The irreversible punch depth, however, could not be identified from a direct observation of the residual impression through AFM because it was too small to the surface roughness. In order to estimate the actual residual stresses in DLC films, Eq. (3) based on the elastic contact mechanics must be modified with the information of the irreversible deformation. However, since the plastic work-hardening of the DLC film is neglected in this study, the final stress equation in Eq. (3) was modified by multiplying the ratio of reversible part to whole stress-induced depth shift. The portion of the reversible depth shift or $h_{\mathrm{res}}^{\mathrm{rev}}/h_{\mathrm{res}}$ were 0.71 and 0.73 for the 0.4 and 0.6 μm-thick DLC films, respectively, and the stress recalculated were -0.92 ± 0.07 and -2.85 ± 0.21 GPa. From a comparison in Fig. 5, the modified equation underestimated the actual stresses slightly and this was attributed to the actual work-hardening behaviors in the DLC films [20]. Although further stress formulation from a viewpoint of irreversibility was impossible without information on the plastic constitutive equation of the DLC film, a new idea was proposed for deriving a stress term from the irreversible punch depth using a previous study on predicting the stress–strain relationship from a flat punch deformation [21]; since a contact pressure is expressed as a power function of the punching depth in plastic deformation region, $h_{\mathrm{res}}^{\mathrm{irr}}$ corresponds to a contact pressure shift ΔP_m. By equating the residual stress induced normal load L_{res} and a product of ΔP_m and punching area, the stress formulation attributed to the irreversibility is possible.

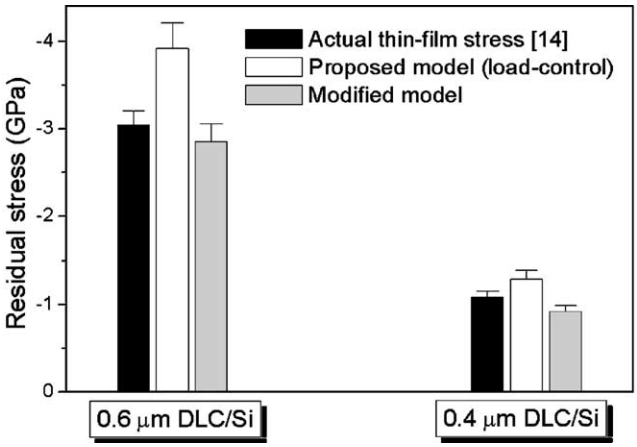

Fig. 5. Comparisons of the recalculated residual stresses for the two DLC films with the actual values measured in the previous study [14].

5. Summary

A shift in the nanoindentation depth by the elastic thin-film stress at a fixed load was analyzed as a reversible surface deformation around a flat punch. The resulting equation was applied to characterize the residual stress in two DLC films but yielded stresses results, 20–30% higher than the actual values of a previous study. This discrepancy was attributed to an influence of an irreversible punch depth and its magnitude was measured from a difference in the contact depth of the as-deposited and free-standing films at a peak load. The thin-film stresses, recalculated after an exclusion of the irreversible depth shift, agreed roughly with the actual stress levels of the DLC films, showing a nil plastic work-hardening behavior. However if an indented material shows a significant work-hardening behavior, the irreversible portion must be formulated into a part of the residual stress using its plastic constitutive equation.

Acknowledgements

This work was supported by the Post-doctoral Fellowship Program of Korea Science & Engineering Foundation (KOSEF).

References

[1] Nix WD. Metall Trans A 1989;20A:2217.
[2] Perry AJ, Sue JA, Martin PJ. Surf Coat Technol 1996;81:17.
[3] James MR, Lu J. In: Handbook of measurement of residual stresses, Society for Experimental Mechanics; 1996, p. 1.

[4] Lee YH, Kwon D. Scripta Mater 2003;49:459.
[5] Doerner MF, Nix WD. J Mater Res 1986;1:601.
[6] Oliver WC, Pharr GM. J Mater Res 1992;7:1564.
[7] LaFontaine WR, Paszkiet CA, Korhonen MA, Li CY. J Mater Res 1991;6:2084.
[8] Zagrebelny AV, Carter CB. Scripta Mater 1997;37:1869.
[9] Tsui TY, Oliver WC, Pharr GM. J Mater Res 1996;11:752.
[10] Bolshakov A, Oliver WC, Pharr GM. J Mater Res 1996;11:760.
[11] Suresh S, Giannakopoulos AE. Acta Mater 1998;46:5755.
[12] Carlsson S, Larsson PL. Acta Mater 2001;49:2179.
[13] Swadener JG, Taljat B, Pharr GM. J Mater Res 2001;16:2091.
[14] Lee YH, Kwon D, Jang JI. Int J Mod Phys B 2003;17:1141.
[15] Lee YH, Ji W, Kwon D. Exp Mech 2004;44:55.
[16] Lee YH, Kwon D. Acta Mater (in press).
[17] Malzbender J, With G. Surf Coat Technol 2000;127:266.
[18] Hong S, Weihs TP, Bravman JC, Nix WD. J Electronic Mater 1990;19:903.
[19] Shen YL. J Mater Res 2003;18:2281.
[20] Schiffmann KI, Hieke A. Wear 2003;254:565.
[21] Yu HI, Imam MA, Rath BB. J Mater Sci 1985;20:636.